

# Deterministic quantum teleportation between distant atomic objects

H. Krauter<sup>1</sup>, D. Salart<sup>1</sup>, C. A. Muschik<sup>2</sup>, J. M. Petersen<sup>1</sup>, H. Shen<sup>1</sup>, T. Fernholz<sup>3</sup>, and E. S. Polzik<sup>1</sup>  
<sup>1</sup> Niels Bohr Institute, Copenhagen University, Blegdamsvej 17, 2100 Copenhagen, Denmark,  
<sup>2</sup> ICFO-Institut de Ciències Fotòniques, Mediterranean Technology Park, 08860 Castelldefels (Barcelona), Spain,  
<sup>3</sup> School of Physics & Astronomy, The University of Nottingham, Nottingham, NG7 2RD, UK

Quantum teleportation is a key ingredient of quantum networks [1, 2] and a building block for quantum computation [3, 4]. Teleportation between distant material objects using light as the quantum information carrier has been a particularly exciting goal. Here we propose and demonstrate a new element of the quantum teleportation landscape, the deterministic continuous variable teleportation between distant material objects. The objects are macroscopic atomic ensembles at room temperature. Entanglement required for teleportation is distributed by light propagating from one ensemble to the other. We demonstrate that the experimental fidelity of the quantum teleportation is higher than that achievable by any classical process. Furthermore, we demonstrate the benefits of deterministic teleportation by teleporting a sequence of spin states evolving in time from one distant object onto another. The teleportation protocol is applicable to other important systems, such as mechanical oscillators coupled to light or cold spin ensembles coupled to microwaves.

Quantum teleportation of discrete [5] and continuous [6] variables is the transfer of a quantum mechanical state without the transmission of a physical system carrying this state. The first experimental teleportation protocols employed light as the carrier of quantum states [7, 8]. Teleportation of atomic states over microns distances has been realized in two experiments using short range interactions between trapped ions [9]. Interspecies teleportation from light onto atoms has been achieved both deterministically for continuous variables [10] and probabilistically for discrete variables [11]. Recently, probabilistic teleportation between two ions [12], atoms [13] and atomic ensembles [14] over a macroscopic distance has been demonstrated. While probabilistic teleportation, in which entanglement is distributed by photon counting [7, 15], is capable of reaching distances of many km [2, 16], the power of continuous variable (cv) teleportation is that it succeeds deterministically in every attempt [8, 10], that it is capable of teleporting complex quantum states [17], and that it can be used in universal quantum computation [4]. Here, we propose and experimentally demonstrate for the first time the deterministic cv teleportation between two distant material objects thus extending the powerful cv teleportation [8, 10, 17] onto atomic memory states. The protocol which succeeds in every attempt allows us to teleport dynamically changing quantum states of collective atomic spins with the bandwidth of tens of Hz.

A quantum teleportation process begins with the creation of a pair of entangled objects. In our experiment these two objects are an atomic ensemble at site B and a photonic wave packet generated by interaction of this ensemble with a driving light pulse (Fig. 1a). The wave packet travels to site A, the location of the atomic ensemble whose state is to be teleported. This step establishes a quantum link between the two locations. Following the interaction of the ensemble A and the wave packet, a measurement is performed on the transmitted light. The results of this measurement are communicated via a classical channel to site B, where they are fed back via local operations on the second entangled object, i.e. the ensemble B, thus completing the process of teleportation. Cv teleportation is described in the language of canonical operators  $x, p$  for atoms and  $y, q$  for light which obey the usual

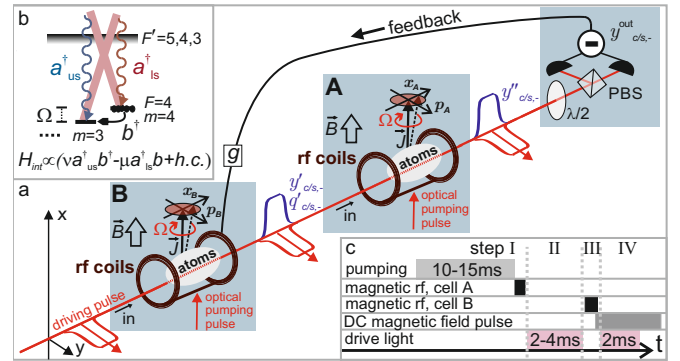


Figure 1: **Teleportation experiment.** (a) The experimental layout. A strong driving pulse propagates first through ensemble B creating the modes  $y', q'$  entangled with B and then through ensemble A whose state is to be teleported. Joint measurements on the modes  $y''$  are performed by polarization homodyning. Teleportation is completed by classical communication of these results to B. More comments in the text. (b) The level scheme and relevant transitions. Classical drive field (thick lines) and quantum fields forming the modes  $y, q$  (wavy lines) are shown, (c) The time line of the experiment. I. Preparation of the input state, II. Entanglement and joint measurement, III. Feedback, IV. Read-out of the teleported state.

commutation relations  $[x, p] = [y, q] = i$ . A generic condition for a cv entangled state for Gaussian states [18] is  $\text{var}(x - y) + \text{var}(p + q) < 2$ . For atomic ensembles, fully spin polarized along the x-axis, canonical operators are scaled dimensionless Cartesian components of the collective spin:  $x = J_y / \sqrt{|\langle J_x \rangle|}$  and  $p = J_z / \sqrt{|\langle J_x \rangle|}$  [18], where  $J_{x,y,z} = \sum_i J_{x,y,z}^i$  (summed over all atoms  $i$ ) is the collective angular momentum of the ensemble. Here, we employ  $^{133}\text{Cs}$  atoms initiated in a fully polarized  $|F = 4, m_F = 4\rangle$  ground state. The usual link between the ladder operator  $b$  for collective atomic excitations [18] of the state  $m_F = 3$  (Fig. 1b) and canonical variables is  $b^\dagger = (x - ip) / \sqrt{2}$ . Atoms are placed in a bias magnetic field along the x-axis, so that in the lab frame the observables  $x \propto J_y$  and  $p \propto J_z$  rotate at Larmor frequency  $\Omega$  (Fig. 1a) according to the atomic Hamiltonian  $H_{\text{Atomic}} = -\Omega (x^2 + p^2) / 2$ . Note that here we use the

parallel orientation of the macroscopic spins of the two ensembles (Fig. 1a) which is optimal for the teleportation protocol. It corresponds to the same sign of the Larmor frequency  $\Omega$  in  $H_{\text{Atomic}}$  for the two ensembles. This is to be compared to [18, 20] where the antiparallel spin orientation, optimal for creating entanglement between two atomic spin ensembles, was used.

The atom-light interaction is shown in Fig. 1b and involves two scattering processes  $H_{int} \propto \nu a_{\text{us}}^\dagger b^\dagger - \mu a_{\text{ls}}^\dagger b + h.c.$  where  $a_{\text{us/ls}}^\dagger$  generate photons in the upper/lower ( $\omega_0 \pm \Omega$ ) sideband modes of the driving field  $\omega_0$ . The interaction  $H_{int}$  contains both essential ingredients of the teleportation protocol, the creation of entanglement (the first term) and a beam-splitter type operation between atoms and photons (the second term) [18, 20]. For our setting the ratio of the two terms is  $\mu/\nu = 1.38$ . The entanglement used in this protocol is between the atomic ensemble B and the light field sent to ensemble A. The photons scattered forward into Larmor frequency sidebands populate the modes relevant for teleportation whose canonical variables  $y_{c,s}$  and  $q_{c,s}$  are  $y_c \cos(\Omega t) + y_s \sin(\Omega t) \propto a_{\text{us}} e^{-i\Omega t} + a_{\text{ls}} e^{i\Omega t} + h.c.$  and similarly for  $q$ . The detailed theory of the protocol is presented in the Supplementary Information (SI), where exact definitions and properties of these modes are given in Eq. (S3,S4). The generic form for them is  $y_{c/s,f} \propto \int_0^T \cos / \sin(\Omega t) f(t) y(t) dt$ , where  $f(t)$  is a function which varies slowly on the time scale of the Larmor period.

The experiment (Fig. 1a) utilizes two room temperature gas ensembles of Cesium atoms in glass cells with spin protecting coating as in [18, 19, 21] placed at a distance of 0.5m. Optical pumping initializes both ensembles into the  $|F = 4, m_F = 4\rangle$  coherent spin state (CSS) state with  $\text{Var}(J_y) \cdot \text{Var}(J_z) = J_x^2/4$  with  $J_x \approx 4N_A$  and  $\langle J_y \rangle = 0$  and  $\langle J_z \rangle = 0$ , corresponding to a vacuum state with variances  $\text{Var}(x) = \text{Var}(p) = 1/2$ . The spin of the ensemble A to be teleported is then displaced with mean values  $\langle x_A \rangle$  and  $\langle p_A \rangle$  by a weak radio-frequency (rf) magnetic field pulse of frequency  $\Omega$  corresponding to the creation of coherent superposition of electronic ground states  $m_F = 3, m_F = 4$  (Fig. 1b).

The layout and the time sequence for teleportation and verification are shown in Fig. 1a,c. A y-polarized, 3ms long 5.6mW light pulse, blue detuned from the  $D_2$  line  $F = 4 \rightarrow 5$  transition by  $\Delta = 850\text{MHz}$  drives the interaction. The forward scattered mode, x-polarized and described by  $y', q'$  is entangled with the collective spin B and co-propagates with the drive light towards the site A. The interaction with the ensemble A leads to partial mapping of its state onto light and is followed by the Bell measurements on the light modes of the upper and lower sidebands performed via polarization homodyning with the driving light acting as the local oscillator yielding  $y_c'' = (y_{\text{us}}'' + y_{\text{ls}}'')/\sqrt{2}$  and  $y_s'' = (q_{\text{ls}}'' - q_{\text{us}}'')/\sqrt{2}$ . The measurements of  $y_c''$  and  $y_s''$  serve as the joint measurement of ensemble A and the light coming from site B as can be seen directly from Eq. (S1) of the SI. Near unity teleportation fidelity can be achieved [23], if the driving fields for A and B ensembles are made time-dependent. However, even with top hat driving pulses a sufficiently high fidelity can be achieved, if an optimal temporal mode for the detected

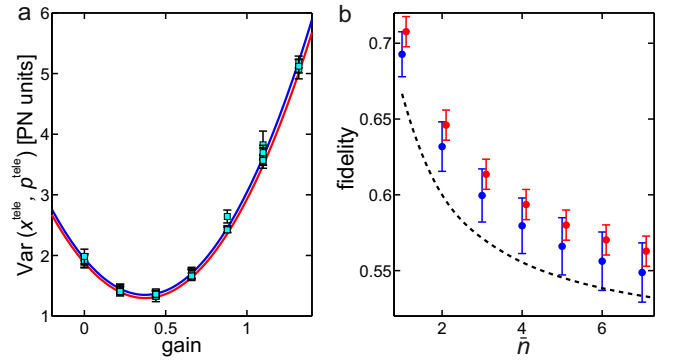


Figure 2: **Teleportation fidelity.** (a) The variances of the teleported state  $\text{Var}(x^{\text{tele}}, p^{\text{tele}})$  in projection (vacuum) noise (PN) units as a function of gain. Several data points for each gain correspond to various input states (the vacuum, the CSS with displacements of 5 in vacuum units and phases 0,  $\pi/4$ ,  $\pi/2$  and CSS with displacement 25 and phase 0). The error bars represent one standard deviation of the atomic variance for 5-10 subsets of 2000 points. (b) Teleportation fidelity as a function of the mean photon number of the Gaussian distribution of the input set of states. Blue curves/points - feedback by rf pulses applied to ensemble B, red curves/points - feedback applied numerically to the read-out results of B (see comments in the text). Black dashed line represents the classical benchmark. For the error bars, the uncertainty of kappa, shot noise, detection efficiency and the quadratic fit of the atomic variance vs gain were taken into account.

homodyne signal is chosen. The optimal readout mode is  $y_{c/s,-} \propto \int_0^T \cos / \sin(\Omega t) e^{-\gamma t} y(t) dt$ , where  $T$  is the pulse duration and  $\gamma$  is the decay rate of the atomic state. Measurements of  $y_{c/s,-}$  are conducted by electronic processing of the photocurrent. The teleportation protocol is completed by sending the measurement results  $y_{c/s,-}^{\text{out}}$  via a classical link to the site B where spin rotations in the y,z plane conditioned on these results are performed using phase and amplitude controlled rf magnetic field pulses at frequency  $\Omega$ . The deterministic character of the homodyne process ensures success of the teleportation in every attempt.

The quantum character of the teleportation is verified by comparing the fidelity of state transfer to the classical benchmark fidelity. More specifically, we perform the teleportation using various sets of coherent spin states of ensemble A with varying  $\langle J_{y,z} \rangle$ , corresponding to displaced vacuum (coherent states) in quantum optical terms, as input states. For such states the individual state transfer fidelity is calculated from the first two moments [23], i.e. the mean values and the variances  $\sigma_x^2 = \text{Var}(x_B^{\text{tele}})$ ,  $\sigma_p^2 = \text{Var}(p_B^{\text{tele}})$ . We then evaluate the average transfer fidelity for sets of coherent input states with a Gaussian distribution of displacements with mean number of spin excitations [22, 23]  $\bar{n} = \langle b^\dagger b \rangle$ . A rigorous classical benchmark fidelity  $(1 + \bar{n})/(1 + 2\bar{n})$  for transmission of such classes of states has been derived in [22]. Demonstration of a fidelity above the classical benchmark signifies the success of quantum teleportation and is equivalent to the ability of the teleportation channel to transfer entangled states. For every input state, 10.000-20.000 teleportations have been

performed with one full cycle of the protocol lasting 20ms. Fig. 2a shows the variance of the teleported states as a function of gain  $g$ . The quadratic dependence of the variances on  $g$  predicted by the model [23] fits the experimental data very well. For a certain range of  $g$  the atomic variances are reduced due to the entanglement of the transmitted light with the ensemble  $B$  [23]. Fig. 2b presents the experimental fidelity (blue dots), which is above the classical benchmark for  $\bar{n} \leq 7$ . The classical feedback conditioned on the Bell measurement result can be applied in two ways. It can be done by performing a displacement operation with an rf pulse applied to ensemble  $B$ , followed by a subsequent verification by the read-out of the atomic state. Alternatively, the verification read-out can be performed first, followed by the displacement operation applied to the result of the measurement numerically (see SI). In theory, those two procedures are equivalent, but in the experiment the resulting fidelity for the latter one is slightly higher (red dots in Fig. 2b) since the application of rf fields required in the former procedure introduces additional technical errors.

The deterministic teleportation can be used for "stroboscopic" teleportation of a sequence of spin states changing at a rate of  $\approx 50$  Hz from  $A$  to  $B$ . To illustrate this attractive feature, we have performed repeated teleportation cycles while varying the amplitude and phase of the input state. The results are presented in Fig. 3. The left column displays the time varying rf field in the picoTesla range which is applied to prepare a new spin state  $A$  in each individual teleportation run, after initializing both ensembles to vacuum between the runs. The central column shows the read-out of the input state evolution of ensemble  $A$  and the right column shows the read-out of the teleported state evolution. The points represent results for individual teleportation runs.

The fidelity of the teleportation can be further improved by using time varying drive pulses [23] and increasing the optical depth of the atomic ensembles. Cv teleportation is capable of teleporting highly non-classical states as shown for teleportation of light modes [17], so it can be expected that deterministic teleportation of an atomic qubit [15] can be performed by developing the present approach. The stroboscopic teleportation of spin dynamics can also be extended towards a true continuous in time teleportation paving the way to teleportation of quantum dynamics and simulations of the interaction between two distant objects which have never interacted directly [24]. Cv atomic teleportation allows for performing quantum sensing at a remote location, spatially separated from the location of the object. This teleportation protocol is, in principle, applicable to other systems described by strongly coupled harmonic oscillators, for example, to mechanical oscillators in a quantum regime coupled to light or cold spin ensembles coupled to microwaves.

### A. Methods Summary

The Larmor precession of the atomic spin oscillators in the bias magnetic field allows us to perform quantum telepor-

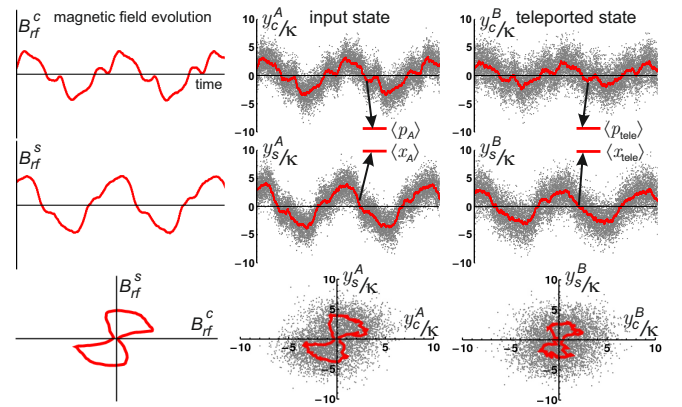


Figure 3: **Teleportation of a sequence of spin states.** Left column - rf magnetic field applied to spin  $A$  with components  $x_A \propto J_y \propto B_{rf}^s, p_A \propto J_z \propto B_{rf}^c$  with the amplitude of  $B_{rf} \approx 1$  picoTesla. Center/right columns - the read-out of the input/teleported spin states  $A/B$  in vacuum units. Every point is one teleportation run with the points taken at the rate of  $\approx 50$ Hz with the whole shown sequence taking  $\approx 200$  sec. The lines present the running average of the points. The first/second row is the  $p_{A,B}/x_{A,B}$  variable and the third row is a two-dimensional plot  $x_{A,B}, p_{A,B}$ . The optimal teleportation gain for this evolution is 0.8 which is seen as a smaller mean amplitude of the teleported evolution compared to the original.

tation with a very large atomic object consisting of  $N_A \approx 10^{11} - 10^{12}$  atoms and to use a strong drive with the number of photons of  $N_{ph} \approx 10^{13} - 10^{14}$ . The relative size of vacuum state fluctuations in a multiparticle ensemble scales as  $N^{-1/2}$ . Therefore all technical fluctuations of spins and light must be reduced to  $\ll 10^{-6}$  before the vacuum state noise level which is the benchmark for cv quantum information processing can be reached. We achieve this by encoding quantum states of atoms and light at the high Larmor frequency  $\Omega = 322$ kHz (the bias magnetic field of  $B \approx 0.9$ G) where technical noise is much lower than at lower frequencies. This allows us to achieve vacuum (projection) noise level for atoms and vacuum (shot) noise level for light. Using the strong driving field also as the local oscillator field for polarization homodyne detection of photonic variables  $y_{c,s}$  allows us to use detectors with nearly unity quantum efficiency.

The calibration of the input atomic spin state, the joint measurement, and the detection of the state teleported onto the spin  $B$  are performed via polarization homodyning measurements of the Stokes operator  $S_2 = (n_{+45} - n_{-45})/2$  given by the difference of photon numbers polarized in  $\pm 45^\circ$  directions (Fig.1) [21, 25]. The measured canonical variable for light is then defined as  $S_2 \approx \sqrt{\Phi}/2 \cdot y$  where  $\Phi$  is the driving field photon flux, which experimentally means that all measurements are normalized to shot noise of light. The photocurrent is analyzed with a lock-in amplifier at  $\Omega$  and further computer processed to obtain measurements of the temporal modes of interest  $y_{c/s,-}$ . Light pulses for teleportation and read-out always pass through both vapour cells (Fig. 1). For the read out of each individual ensemble the other ensemble is detuned from the atom-light interaction by briefly detuning the  $B$  field in the respective cell. For off-resonant light

well below saturation used here, the linear transformation of light variables after dispersive interaction with atoms is given by [20, 25]:

$$y_{c/s,-} = \kappa \cdot p/x + c_y \cdot y_{c/s,f_y}^{\text{in}} + c_q \cdot q_{s/c,f_q}^{\text{in}} + c_N \cdot F_{p,x}. \quad (1)$$

Here, the first term is a contribution of the atomic spin variable due to Faraday rotation of light polarization, the second term is proportional to the input value of the light quadrature  $y$  of the temporal mode  $f_y$  and the third term is the contribution of the other quadrature of input light  $q$  of temporal mode  $f_q$  resulting from back action of light on atoms [23]. All input light modes are always in a coherent or vacuum state with  $\text{Var}(y_{c/s,f_y}^{\text{in}}) = \text{Var}(q_{s/c,f_q}^{\text{in}}) = 1/2$ . The last term in Eq. 1 describes additional noise arising from atomic decoherence with  $\text{Var}(F_{p,x}) = m/2$  with  $m = 1.3$  found from the atomic spin relaxation [26]. The value of the interaction constant  $\kappa$  is found by calibrating the Faraday rotation caused by the ensemble [20]. The constants  $c_y$  and  $c_q$  are determined by sending light with displacements of  $\langle y_{c/s,f_y}^{\text{in}} \rangle$  and  $\langle q_{s/c,f_q}^{\text{in}} \rangle$ , storing it in the atomic medium, then reading it out onto another pulse  $\langle y_{c/s,-}^{\text{out}} \rangle$  and measuring the ratios. The values for  $c_y$ ,  $c_q$  and  $c_N$  can also be calculated from the model [23] based on three experimental parameters: the total transverse decay rate of the atomic spin state  $\gamma$ , the contribution of spin decoherence (spontaneous emission, collisions and inhomogeneity of the magnetic field) to this decay rate  $\gamma_{\text{extra}}$  and  $Z^2 = (\mu + \nu)/(\mu - \nu)$ .  $Z^2 = 6.3$  is calculated from Clebsch-Gordon coefficients for the atomic transitions and experimentally verified [19]. For 5.6mW read out pulses of 2ms duration and room temperature Cs vapor pressure (effective resonant optical depth of 34 for 22mm long cells)  $\gamma = 99.3 \pm 0.2 \text{sec}^{-1}$  and  $\gamma_{\text{extra}} = 26.3 \pm 0.2 \text{sec}^{-1}$  have been measured. A unitary contribution to the decay  $\gamma - \gamma_{\text{extra}}$  is due to the collective coupling  $H_{\text{int}}$ , which describes the rate of entanglement generation and the beam splitter interaction [23] and depends on the optical depth of the ensemble, the optical detuning, and the intensity of the driving field. The measured values of  $\kappa$ ,  $c_y$ ,  $c_q$  agree very well with the predictions of the model [23] and are  $\kappa = 0.87$ ,  $c_y = 0.93$ ,  $c_q = 0.50$  for our teleportation setting. The last coefficient in the read-out equation can be found from the measured parameters as  $c_N = c_q \cdot \sqrt{2 \cdot \gamma_{\text{extra}} / (\gamma - \gamma_{\text{extra}})} / Z = 0.17$ . For the atomic state reconstruction the detection efficiencies including optical losses  $\eta_B = 0.80 \pm 0.03$  and  $\eta_A = 0.89 \pm 0.03$  for ensem-

bles A/B are taken into account.

Using Eq.1 the mean values of the input states of ensemble A are found from measurements of light variables as  $\langle x_A \rangle = \langle y_{c,-}^A \rangle / \kappa$ ,  $\langle p_A \rangle = \langle y_{s,-}^A \rangle / \kappa$  and their variances as  $\text{Var}(x_A) = (\text{Var}(y_{c,-}^A) - c_y^2/2 - c_q^2/2 - c_N^2 m/2) / \kappa^2$ ,  $\text{Var}(p_A) = (\text{Var}(y_{s,-}^A) - c_y^2/2 - c_q^2/2 - c_N^2 m/2) / \kappa^2$ .

The prepared atomic input states are found to be very close to ideal CSS with  $\text{Var}(x_A) = \text{Var}(p_A) = (1.03 \pm 0.03) \cdot 1/2$ , which confirms the validity of the read-out procedure. After each teleportation sequence, the mean values and the variances  $\langle x_B^{\text{tele}} \rangle$ ,  $\langle p_B^{\text{tele}} \rangle$ ,  $\text{Var}(x_B^{\text{tele}})$ ,  $\text{Var}(p_B^{\text{tele}})$  of the spin state of the target ensemble B are found in the same way from the read-out of the verification pulse  $y_{c/s,-}^B$ . For CSS input states with displacements of 0, 5, 25, 160 in canonical units and phases 0,  $\pi/4$ ,  $\pi/2$  in  $x, p$  space, the variance of the teleported state showed no dependence on the displacement. The experimental fidelity is determined using a standard method of calculation of the state overlap [23]. Optimization of the teleportation protocol has been performed by varying the drive pulse duration  $T$ , the measured temporal mode of light, and the gain for the classical feedback. The optimal read-out mode was always found with an exponential decay rate equal to the spin decay  $\gamma$  as expected from the model.

## I. ACKNOWLEDGEMENTS

We gratefully acknowledge discussions with J. I. Cirac, K. Hammerer and D. V. Vasilyev. This work was supported by the ERC grants INTERFACE and QUAGATUA, the Danish National Science Foundation Center QUANTOP, the DARPA program QUASAR, the Alexander von Humboldt Foundation, TOQATA (FIS2008-00784) and the EU projects QESSENCE, MALICIA and AQUTE.

## II. AUTHOR CONTRIBUTIONS

H.K., D.S., J.M.P, H.S. and T.F. performed the experiment. The theoretical model has been developed by C.A.M. H.K, C.A.M., D.S. and E.S.P have written the paper. E.S.P supervised the project.

- 
- [1] Briegel, H.-J., Dür, W., Cirac, J. I. & Zoller, P. Quantum Repeaters: The Role of Imperfect Local Operations in Quantum Communication. *Physical Review Letters*, **81**, 5932–5935 (1998).
- [2] de Riedmatten, H. *et al.* Long Distance Quantum Teleportation in a Quantum Relay Configuration *Physical Review Letters*, **92**, 47904 (2004).
- [3] Gottesman, D. & Chuang, I.L. Demonstrating the viability of universal quantum computation using teleportation and single-qubit operations *Nature*, **402**, 390–393 (1999).

- [4] Gottesman, D., Kitaev, A., Preskill, J. Encoding a qubit in an oscillator. *Physical Review A*, **64**, 012310 (2001).
- [5] Bennett, C. H. *et al.* Teleporting an unknown quantum state via dual classical and Einstein-Podolsky-Rosen channels *Physical Review Letters*, **70**, 1895–1899 (1993).
- [6] Vaidman, L. Teleportation of quantum states *Physical Review A*, **49**, 1473–1476 (1994).
- [7] Bouwmeester, D. *et al.*, A Experimental quantum teleportation *Nature*, **390**, 575–579 (1997).
- [8] Furusawa, A. *et al.* Unconditional Quantum Teleportation *Sci-*

- ence , **282**, 706–709 (1998).
- [9] Riebe, M. *et al.* Deterministic quantum teleportation of atomic qubits *Nature*, **429**, 737–739 (2004). Barret, M.D. *et al.* Deterministic quantum teleportation with atoms *Nature*, **429**, 734–737 (2004).
- [10] Sherson, J. *et al.* Quantum teleportation between light and matter *Nature*, **443**, 557–560 (2006).
- [11] Chen, Y.A. *et al.* Memory-built-in quantum teleportation with photonic and atomic qubits *Nature Physics*, **4**, 103–107 (2008).
- [12] Olmschenk, S. *et al.* Quantum Teleportation Between Distant Matter Qubits *Science*, **323**, 486–489 (2009).
- [13] Nölleke, C., Neuzner, A., Reiserer, A., Hahn, C., Rempe, G., & Ritter, S. Efficient teleportation between remote single-atom quantum memories. Preprint available at <http://arxiv.org/abs/1212.3127>.
- [14] Bao X-H. *et al.* Quantum teleportation between remote atomic-ensemble quantum memories *Proceedings of the National Academy of Sciences of the United States of America*, **109**, 20347–20351 (2012).
- [15] Duan, L.M., Lukin, M.D., Cirac, J.I. & Zoller, P. Long-distance quantum communication with atomic ensembles and linear optics *Nature*, **414**, 413–418 (2001).
- [16] Ma, X.S. *et al.* Quantum teleportation over 143 kilometres using active feed-forward *Nature*, **489**, 269–273 (2012).
- [17] Lee, N. *et al.* Teleportation of Nonclassical Wave Packets of Light *Science*, **332**, 330–333 (2011).
- [18] Hammerer, K., Sørensen, A.S. & Polzik, E.S. Quantum inter-  
face between light and atomic ensembles *Reviews of Modern Physics*, **82**, 1041–1093 (2010).
- [19] Wasilewski, W. *et al.* Generation of two-mode squeezed and entangled light in a single temporal and spatial mode *Optics Express*, **17**, 14444–14457 (2009).
- [20] Krauter, H. *et al.* Entanglement Generated by Dissipation and Steady State Entanglement of Two Macroscopic Objects *Physical Review Letters*, **107**, 080503 (2011).
- [21] Sherson, J., Julsgaard, B. & Polzik, E.S. Deterministic Atom-Light Quantum Interface *Advances in Atomic, Molecular, and Optical Physics*, **54**, 81–130 (2006).
- [22] Hammerer, K., Wolf, M.M., Polzik, E.S. & Cirac, J.I. Quantum benchmark for storage and transmission of coherent states *Physical Review Letters*, **94**, 150503 (2005).
- [23] More details are given in the Supplementary information.
- [24] Muschik, C.A., Hammerer, K., Polzik, E.S. & Cirac J.I. Quantum Teleportation of Dynamics and Effective Interactions Between Remote Systems arXiv:1304.0319 (2013).
- [25] Muschik, C.A. *et al.* Robust entanglement generation by reservoir engineering *Journal of Physics B: Atomic, Molecular and Optical Physics*, **45**, 124021 (2012).
- [26] Vasilyev, D.V., Hammerer, K., Korolev, N. & Sørensen, A.S. Quantum Noise for Faraday Light Matter Interfaces *Journal of Physics B: Atomic, Molecular and Optical Physics* **45** 124007 (2012).

---

### Supplemental Information

In the following, we provide additional information on the the read-out of the atomic spin state and the protocol used for teleportation. In Sec. 1, we discuss the input-output relations for the interaction of a single cell with light. These equations are the basis for the read-out which is used for verification. In Sec. 2, we explain the teleportation scheme, state the corresponding input-output relations for atoms and light and calculate the attainable fidelity.

#### 1. Light-matter interaction

We are interested in reading out the spin state of an atomic ensemble, which is described in terms of bosonic operators  $x$  and  $p$ . This information is mapped to a coherent light field. The interaction of light with atoms, which are rotating in a magnetic field with a Larmor frequency  $\Omega$  leads to temporally modulated light modes. More specifically, the atomic quadratures  $x$  and  $p$  are mapped to  $\sin(\Omega t)$  and  $\cos(\Omega t)$  modulated light modes respectively, which can be accessed individually. As explained below, we consider here specific light modes with an exponentially falling slowly varying envelope on top of the fast sine/cosine modulation. The relevant input-output relation for these read-out modes are given by

$$\begin{pmatrix} y_{c,-} \\ y_{s,-} \end{pmatrix} = \kappa \begin{pmatrix} p^{\text{in}} \\ x^{\text{in}} \end{pmatrix} + c_y \begin{pmatrix} y_{c,f_y}^{\text{in}} \\ y_{s,f_y}^{\text{in}} \end{pmatrix} + c_q \begin{pmatrix} -q_{s,f_q}^{\text{in}} \\ q_{c,f_q}^{\text{in}} \end{pmatrix} + c_N \begin{pmatrix} F_p^{\text{in}} \\ F_x^{\text{in}} \end{pmatrix}. \quad (\text{S.1})$$

These equations include atomic decay. The first term on the right side is the desired atomic signal. The second and third term on the right represent contributions of the light field. The first subscript of the photonic operators refers to the fast modulation (i.e. modulation with  $\sin(\Omega t)$  or  $\cos(\Omega t)$ ), while the second subscript refers to the mode function of the slowly varying envelope (as explained below).  $F_x^{\text{in}}$  and  $F_p^{\text{in}}$  are atomic noise operators,  $\kappa$ ,  $c_y$ ,  $c_q$  and  $c_N$  are real coefficients and are given by Eqs. (S.6) below.

The interaction between atoms and light is governed by the Hamiltonian  $H = H_A + H_L + H_{\text{int}}$ , where  $H_L$  represents the free propagation of the light field along  $z$  and  $H_A$  is the free Hamiltonian of the atomic system. More specifically,  $H_A = -\Omega(x^2 + p^2)/2$ , describes the Larmor precession with Larmor frequency  $\Omega$  of the atoms in the magnetic field. The interaction Hamiltonian is a combination of a passive (beam splitter-) part  $H_{\text{BS}}$ , which preserves the number of excitations in the

system and an active (two mode squeezing) part  $H_{\text{TMS}}$ , which creates entanglement between atoms and light,

$$H_{\text{int}} = \sqrt{2\gamma_s}(\mu H_{\text{BS}} - \nu H_{\text{TMS}}) = \sqrt{2\gamma_s} \left( Zpq(0) + \frac{1}{Z}xy(0) \right), \quad (\text{S.2})$$

where  $\mu = \frac{1}{2} \left( Z + \frac{1}{Z} \right)$ ,  $\nu = \frac{1}{2} \left( Z - \frac{1}{Z} \right)$ . Here, we assumed a pointlike atomic ensemble which is located at the origin  $z = 0$ . The light field is described in terms of spatially localized modes [1–3],

$$\begin{aligned} y(z) &= \frac{1}{4\pi} \int_b d\omega \left( a(\omega) e^{-i(\omega_0 - \omega)z/c} + H.C. \right), \\ q(z) &= \frac{-i}{4\pi} \int_b d\omega \left( a(\omega) e^{-i(\omega_0 - \omega)z/c} - H.C. \right), \end{aligned} \quad (\text{S.3})$$

where  $c$  is the speed of light and  $b$  is the bandwidth of the applied laser field with central frequency  $\omega_0$ . The canonical variables  $y(z)$  and  $q(z)$  obey the commutation relation  $[y(z), q(z')] = c\delta(z - z')$ . The width of the delta function is on the order of  $c/b$ . In the following, we write the time argument explicitly ( $y(z, t)$ ,  $q(z, t)$ ) and perform a variable transformation  $\bar{y}(\xi, t) = y(ct - \xi, t)$  on the spatial argument of the light-field operators. The transformed operators describe the light field in the moving frame (see for example [3, 4]). Using this description, integrated light modes can be defined by considering an integral over the individual pieces of the light pulse with temporally varying weighting functions (see Eq. (S.4) and Eq. (S.5)).

We derive the input-output relations for the light-matter interaction given by Eq. (S.2) in the limit  $\Omega T \gg 1$ , where  $T$  is the total interaction time. Contributions which are on the order of  $(\Omega T)^{-1}$  are neglected, which is a very good approximation for the experimental parameters considered here (compare [3, 5, 6]). We include undesired noise processes, which lead to a decay of the transverse atomic spin at a rate  $\gamma_{\text{extra}}$ . In the presence of noise, the optimal slowly varying envelope for the read-out is an exponentially falling mode  $e^{-\gamma t}$ , where  $\gamma = \gamma_s + \gamma_{\text{extra}}$ . In the experiment, the exponentially falling sine and cosine modulated light modes

$$\begin{pmatrix} y_{c,-} \\ y_{s,-} \end{pmatrix} = \frac{2\sqrt{\gamma}}{\sqrt{1 - e^{-2\gamma T}}} \int_0^T dt e^{-\gamma t} \begin{pmatrix} \cos(\Omega t) \\ \sin(\Omega t) \end{pmatrix} \bar{y}(ct, T) \quad (\text{S.4})$$

are measured. The corresponding input-output relations are given by Eq. (S.1) above. The light and noise modes appearing in this equation are defined by

$$\begin{aligned} \begin{pmatrix} y_{c,f_y}^{\text{in}} \\ y_{s,f_y}^{\text{in}} \end{pmatrix} &= \frac{1}{\sqrt{N_y}} \int_0^T dt f_y(t) \begin{pmatrix} \cos(\Omega t) \\ \sin(\Omega t) \end{pmatrix} \bar{y}(ct, 0), \\ \begin{pmatrix} q_{s,f_q}^{\text{in}} \\ q_{c,f_q}^{\text{in}} \end{pmatrix} &= \frac{1}{\sqrt{N_q}} \int_0^T dt f_q(t) \begin{pmatrix} \sin(\Omega t) \\ \cos(\Omega t) \end{pmatrix} \bar{q}(ct, 0), \\ \begin{pmatrix} F_p^{\text{in}} \\ F_x^{\text{in}} \end{pmatrix} &= \frac{1}{\sqrt{N_N}} \int_0^T dt f_N(t) \begin{pmatrix} f_p(t) \\ f_x(t) \end{pmatrix}, \end{aligned} \quad (\text{S.5})$$

where  $f_x(t)$  and  $f_p(t)$  are atomic noise operators with  $\langle f_x(t) \rangle = \langle f_p(t) \rangle = 0$  and  $\langle f_x(t) f_x(t') \rangle = \langle f_p(t) f_p(t') \rangle = \frac{m}{2} \delta(t - t')$ . Accordingly,  $\text{var}(F_x^{\text{in}}) = \text{var}(F_p^{\text{in}}) = m/2$ . For the interaction Hamiltonian, given by Eq. (S.2), one obtains  $m = 1.3$  [7, 8]. The modulating functions  $f_y$ ,  $f_q$  and  $f_N$  read

$$\begin{aligned} f_y(t) &= \frac{1}{\sqrt{1 - e^{-2\gamma T}}} \left( \left[ 2\sqrt{\gamma} - \frac{\gamma_s}{\sqrt{\gamma}} \right] e^{-\gamma t} + \frac{\gamma_s}{\sqrt{\gamma}} e^{-2\gamma T} e^{\gamma t} \right), \\ f_q(t) &= Z^2 \frac{\gamma_s}{\sqrt{\gamma}} \frac{1}{\sqrt{1 - e^{-2\gamma T}}} (e^{-\gamma t} - e^{-2\gamma T} e^{\gamma t}), \\ f_N(t) &= Z \frac{\sqrt{\gamma_s \gamma_{\text{extra}}}}{\sqrt{\gamma}} \frac{1}{\sqrt{1 - e^{-2\gamma T}}} (e^{-\gamma t} - e^{-2\gamma T} e^{\gamma t}), \end{aligned}$$

with

$$N_y = \frac{1}{2} \int_0^T dt f_y(t)^2, \quad N_q = \frac{1}{2} \int_0^T dt f_q(t)^2, \quad N_N = \int_0^T dt f_N(t)^2.$$

The coefficients appearing in Eq. (S.1) are given by

$$\kappa = \frac{Z\sqrt{\gamma_s}}{\sqrt{2\gamma}} \sqrt{1 - e^{-2\gamma T}}, \quad c_y = \sqrt{N_y}, \quad c_q = \sqrt{N_q}, \quad c_N = \sqrt{N_N}. \quad (\text{S.6})$$

It is instructive to consider the limiting case of large  $Z^2 \gg 1$ , with  $\gamma_s T Z^2 = \text{const}$ . In this limit,  $\mu = \nu$  and we obtain a quantum non demolition (QND) interaction with  $H_{\text{int}} \propto pq$ . In the absence of decay, the coefficients of the input-output relation Eq. (S.1) become

$$\kappa = Z\sqrt{\gamma T}, \quad c_y = 1, \quad c_q = \kappa^2/\sqrt{3}, \quad c_N = 0. \quad (\text{S.7})$$

In this case, the readout equations take a form extensively used previously [3, 5]

$$\begin{pmatrix} y_{c,-} \\ y_{s,-} \end{pmatrix} = \begin{pmatrix} y_{c,-}^{\text{in}} \\ y_{s,-}^{\text{in}} \end{pmatrix} + \kappa \begin{pmatrix} p^{\text{in}} \\ x^{\text{in}} \end{pmatrix} + \frac{\kappa^2}{\sqrt{3}} \begin{pmatrix} -q_{s,f_q}^{\text{in}} \\ q_{c,f_q}^{\text{in}} \end{pmatrix}. \quad (\text{S.8})$$

Eq. (S.2) shows that the interaction between the atomic ensemble and the light field leads to entanglement between these two systems. The exact form of the entangled modes and the degree of entanglement depends on the specific parameters characterizing the interaction,  $\gamma_s$  and  $Z$ , and on the added noise. In essence, the underlying physics can be understood by considering the special case of an Einstein-Podolski-Rosen-entangled state [9] and the nonlocal variables  $x_- = (x_{\text{atom}} - x_{\text{light}})/\sqrt{2}$  and  $p_+ = (p_{\text{atom}} + p_{\text{light}})/\sqrt{2}$ , where  $x_{\text{atom}}, p_{\text{atom}}$  and  $x_{\text{light}}, p_{\text{light}}$  are appropriate quadratures of the atomic ensemble and a suitable integrated light mode. The inequality  $\text{var}(x_-) + \text{var}(p_+) < 1$  indicates that the two systems are entangled. It certifies the existence of intersystem correlations which are stronger than classically allowed. For a perfectly entangled state  $\text{var}(x_+) + \text{var}(p_-) = 0$ . In this case, the  $x$ -quadratures of the two systems are perfectly correlated. If a measurement of the atomic  $x$ -quadrature yields the value  $x_1$ , then the corresponding measurement on the photonic system yields also  $x_1$ . The  $p$ -quadratures are anti-correlated. If the value  $p_1$  is obtained in a measurement of the atomic ensemble, the corresponding measurement on the light field yield  $-p_1$ .

## 2. Teleportation scheme

In this section, we discuss the teleportation scheme. In Sec. 2 a, we explain the basic working principle of the protocol and provide the corresponding input-output relations. In Sec. 2 b, we compute the teleportation fidelity.

### a. Protocol and input-output relations

A standard teleportation scheme involving the three parties Alice, Bob and Charlie consists of the following three steps, which allow Alice to teleport a quantum state provided by Charlie to Bob. (i) Alice and Bob establish an entangled link, which is shared between the two remote parties. (ii) Alice performs a Bell measurement on her part of the entangled state shared with Bob and an unknown quantum state prepared by Charlie. (iii) Alice uses a classical channel to communicate the measurement outcome to Bob, who performs a local operation on his quantum state conditioned on Alice's result.

The setup used here is shown in Fig.1a in the main text. The quantum state prepared by Charlie (on Alice's side) is stored in ensemble A. This state is teleported to ensemble B, which represents Bob, while the light field in  $x$ -polarization plays the role of Alice. Step (i) in the standard protocol outlined above corresponds to the interaction between the light field and the first atomic ensemble which results in an entangled state. The distribution of entanglement between the two remote sites is realized by means of the free propagation of the photonic state. Step (ii) corresponds to the interaction of the light field with the second ensemble and the subsequent measurement of the  $y$ -quadrature of the transmitted light by means of homodyne detection. Step (iii) is implemented in the form of a feedback operation realizing a conditional displacement on ensemble B using radio-frequency magnetic fields. Note that the measurement result in step (ii) is probabilistic and leads therefore to a random displacement of Bob's state in phase space. Since the measurement result is known, the resulting  $x$ , and  $p$ -quadratures of ensemble B are known such that a conditional displacement operation can be applied in step (iii) which shifts Bob's state to the desired coordinates in phase space. In principle, it is not necessary to perform the displacement operation on ensemble B. Instead, the outcome of the measurement in step (ii) can also be communicated to Bob who uses this information to locate the quantum state correctly in phase space when reading it out.

The measured values of  $y_{c,-}^{\text{out}}$  and  $y_{s,-}^{\text{out}}$  are fed back onto ensemble B as explained above. Due to symmetry reasons,

applying equal gain factors  $g_x = g_p = g$  is optimal. This yields

$$\begin{pmatrix} x_B^{\text{tele}} \\ p_B^{\text{tele}} \end{pmatrix} = \bar{c}_B \begin{pmatrix} x_B^{\text{in}} \\ p_B^{\text{in}} \end{pmatrix} + \bar{c}_A \begin{pmatrix} x_A^{\text{in}} \\ p_A^{\text{in}} \end{pmatrix} + \bar{c}_{N,B} \begin{pmatrix} F_{x_B}^{\text{in}} \\ F_{p_B}^{\text{in}} \end{pmatrix} + \bar{c}_{N,A} \begin{pmatrix} F_{x_A}^{\text{in}} \\ F_{p_A}^{\text{in}} \end{pmatrix} \\ + \bar{c}_y \begin{pmatrix} y_{s,\bar{f}_y}^{\text{in}} \\ y_{c,\bar{f}_y}^{\text{in}} \end{pmatrix} + \bar{c}_q \begin{pmatrix} q_{c,\bar{f}_q}^{\text{in}} \\ -q_{s,\bar{f}_q}^{\text{in}} \end{pmatrix}. \quad (\text{S.9})$$

The modes appearing in this equation are defined as in Eq. (S.5) with

$$\begin{aligned} \bar{f}_{N,B} &= \sqrt{2\gamma_{\text{extra}}}(e^{-\gamma(T-t)} + \frac{Z\sqrt{2\gamma_s\gamma}g}{\sqrt{1-e^{-2\gamma T}}}\int_t^T dt' e^{-\gamma(2t'-t)}[1-2\gamma_s(t'-t)]), \\ \bar{f}_{N,A} &= \frac{Z\sqrt{\gamma_s\gamma_{\text{extra}}}}{\sqrt{\gamma}}\frac{g}{\sqrt{1-e^{-2\gamma T}}}(e^{-\gamma t} - e^{-2\gamma T}e^{\gamma t}), \\ \bar{f}_y &= -\frac{\sqrt{2\gamma_s}}{Z}e^{-\gamma(T-t)} + \frac{\gamma_s}{\sqrt{\gamma}}\frac{g}{\sqrt{1-e^{-2\gamma T}}}\left\{\frac{2\gamma}{\gamma_s}e^{-\gamma t} - [e^{-\gamma t}(2 - \frac{\gamma_s}{\gamma}) \right. \\ &\quad \left. - e^{-2\gamma T}e^{\gamma t}(2 - \frac{\gamma_s}{\gamma} - 2\gamma_s(T-t))\right\}, \\ \bar{f}_q &= \sqrt{2\gamma_s}Z\{e^{-\gamma(T-t)} + \frac{Zg\sqrt{\gamma_s}}{\sqrt{2\gamma}\sqrt{1-e^{-2\gamma T}}}[e^{-\gamma t}(2 - \frac{\gamma_s}{\gamma}) \\ &\quad - e^{-2\gamma T}e^{\gamma t}(2 - \frac{\gamma_s}{\gamma} - 2\gamma_s(T-t))\}. \end{aligned}$$

The corresponding normalization factors read

$$\bar{N}_{N,B/A} = \int_0^T dt \bar{f}_{N,B/A}(t)^2, \quad \bar{N}_{y/q} = \frac{1}{2} \int_0^T dt \bar{f}_{y/q}(t)^2.$$

and the coefficients appearing in Eq. (S.9) are given by

$$\begin{aligned} \bar{c}_B &= e^{-\gamma T} + \frac{gZ\sqrt{\gamma_s}}{\sqrt{2\gamma}} \left( \sqrt{1-e^{-2\gamma T}}[1 - \frac{\gamma_s}{\gamma}] + 2\gamma_s T \frac{e^{-2\gamma T}}{\sqrt{1-e^{-2\gamma T}}} \right), \\ \bar{c}_A &= \frac{gZ\sqrt{\gamma_s}}{\sqrt{2\gamma}} \sqrt{1-e^{-2\gamma T}}, \\ \bar{c}_{N,B} &= \sqrt{\bar{N}_{N,B}}, \quad \bar{c}_{N,A} = \sqrt{\bar{N}_{N,A}}, \quad \bar{c}_y = \sqrt{\bar{N}_y}, \quad \bar{c}_q = \sqrt{\bar{N}_q}. \end{aligned}$$

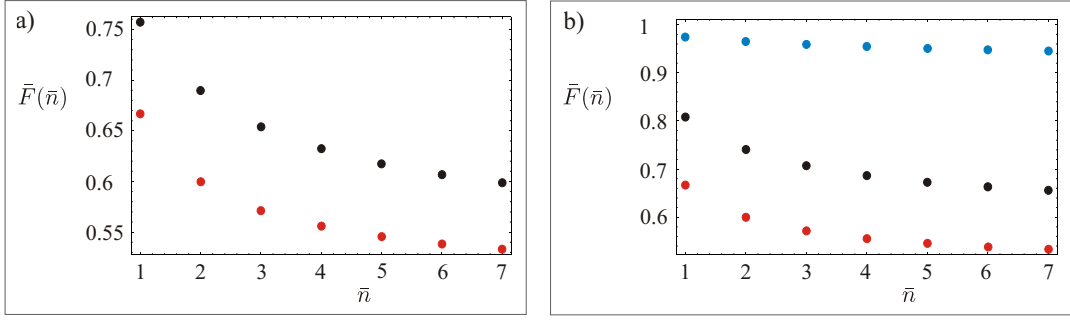
All coefficients and mode functions in the input-output equation for the final atomic state Eq. (S.9) carry a bar in order to avoid confusion with the coefficients and mode functions appearing in the readout equation Eq. (S.1) in Sec. 1.

### b. Teleportation fidelity

The performance of the protocol is assessed using the average fidelity with respect to a Gaussian distribution of coherent input states as figure of merit. The fidelity  $F = |\langle \Psi_B^{\text{tele}} | \Psi_B^{\text{opt}} \rangle|^2$  is given by the overlap of the final atomic state in ensemble B (Bob's state),  $|\Psi_B^{\text{tele}}\rangle$ , which is described by  $x_B^{\text{tele}}$  and  $p_B^{\text{tele}}$  and the optimal final state which is defined by the initial state in ensemble A (Charlie's state)  $x_A^{\text{in}}$ ,  $p_A^{\text{in}}$ . For a given coherent input state with mean values  $\langle x_A \rangle$  and  $\langle p_A \rangle$  (and variances  $\text{var}(x_A) = \text{var}(p_A) = 1/2$ ), the single-shot fidelity is given by

$$F(\langle x_A \rangle, \langle p_A \rangle) = 2 \frac{e^{-\frac{(|\langle x_A \rangle| - |\langle x_B^{\text{tele}} \rangle|)^2}{1+2\text{var}(x_B^{\text{tele}})}}}{\sqrt{(1+2\text{var}(x_B^{\text{tele}}))}} \frac{e^{-\frac{(|\langle p_A \rangle| - |\langle p_B^{\text{tele}} \rangle|)^2}{1+2\text{var}(p_B^{\text{tele}})}}}{\sqrt{(1+2\text{var}(p_B^{\text{tele}}))}},$$





Supplementary figure S.1: Average teleportation fidelity  $\bar{F}(\bar{n})$  for optimal gain  $g$  versus width of the distribution of input states  $\bar{n}$ . The lowest (red) line in both panels represents the classical benchmark. a) Teleportation fidelity for the measured experimental parameters (see methods). b) Maximum teleportation fidelity in the absence of losses. The curve in the middle (black) shows the attainable teleportation fidelity for the interaction used in the experiment ( $Z = 2.5$ ). The upmost curve (blue) depicts the QND-fidelity (for  $Z \rightarrow \infty$ ,  $\gamma_s T Z^2 = \text{const}$ ) for exponentially shaped driving pulses (compare text, Sec. 2 b).

such that the average fidelity  $\bar{F}(\bar{n})$  with respect to a Gaussian distribution with width  $\bar{n}$ ,

$$\bar{F}(\bar{n}) = \frac{1}{2\pi\bar{n}} \iint_{-\infty}^{\infty} d\langle x_A \rangle d\langle p_A \rangle F(\langle x_A \rangle, \langle p_A \rangle) e^{-\frac{\langle x_A \rangle^2 + \langle p_A \rangle^2}{2\bar{n}}}, \quad (\text{S.10})$$

$$= \frac{\sqrt{2}}{\sqrt{1 + 2\text{var}(x_B^{\text{tele}}) + 2\bar{n} \left(1 - \left|\frac{\langle x_B \rangle}{\langle x_A \rangle}\right|\right)^2}} \frac{\sqrt{2}}{\sqrt{1 + 2\text{var}(p_B^{\text{tele}}) + 2\bar{n} \left(1 - \left|\frac{\langle p_B \rangle}{\langle p_A \rangle}\right|\right)^2}}.$$

Both ensembles are initialized in a coherent spin state with  $\langle x_B \rangle = \langle x_A \rangle = 0$  and  $\langle x_B^2 \rangle = \langle x_A^2 \rangle = 1/2$ . The photonic modes are also initially in the vacuum state, such that

$$\begin{aligned} |\langle x_B \rangle / \langle x_A \rangle| &= |\langle p_B \rangle / \langle p_A \rangle| = \bar{c}_A, \\ \text{var}(x_B^{\text{tele}}) &= \text{var}(p_B^{\text{tele}}) = \frac{1}{2} (\bar{c}_B^2 + \bar{c}_A^2 + m\bar{c}_{N,B}^2 + m\bar{c}_{N,A}^2 + \bar{c}_y^2 + \bar{c}_q^2). \end{aligned}$$

Fig. (S1) shows the average teleportation fidelity  $\bar{F}(\bar{n})$  in comparison to the classical limit  $F_{\text{clas}} = (1 + \bar{n}) / (1 + 2\bar{n})$ , which cannot be surpassed by classical means [10–12]. This figure also displays the average fidelity which can be achieved using a QND-interaction (i.e. for very large detuning, see Sec. 1) if the classical driving pulses are modulated in time. These results have been obtained by considering different exponential functions  $f_B(t) \propto e^{f_B t}$  and  $f_A(t) \propto e^{f_A t}$  for the pulse shape of the classical field in the first and second interaction. The fidelity is optimized with respect to  $f_B$  and  $f_A$ . Fig. (S1) b shows that fidelities close to one can be obtained in principle.

- 
- [1] A. Silberfarb, I.H. Deutsch, Phys. Rev. A **68**, 13817 (2003).  
 [2] L.B. Madsen, K. Mølmer, Phys. Rev. A, **70**, 052324 (2004).  
 [3] K. Hammerer, E.S. Polzik, and J.I. Cirac, Phys. Rev. A **72**, 052313 (2005).  
 [4] C.A. Muschik, H. Krauter, K. Jensen, J.M. Petersen, J.I. Cirac, and E.S. Polzik, J. Phys. B: At. Mol. Opt. Phys. **45**, 124021 (2012).  
 [5] K. Hammerer, A. Sørensen, and E.S. Polzik, Rev. Mod. Phys. **82**, 1041 (2010).  
 [6] C.A. Muschik, E.S. Polzik, and J.I. Cirac, Phys. Rev. A **83**, 052312 (2011).  
 [7] D. V. Vasilyev, K. Hammerer, N. Korolev, A. S. Sorensen, J. Phys. B: At. Mol. Opt. Phys. **45**, 124007 (2012).  
 [8] D. V. Vasilyev and Klemens Hammerer, personal communication.  
 [9] A. Einstein, B. Podolsky and N. Rosen, Phys. Rev. **47**, 777 (1935).  
 [10] A. Furusawa, J.L. Sørensen, S. L. Braunstein, C. A. Fuchs, H.J. Kimble and E.S. Polzik, Science **282**, 706 (1998).  
 [11] S.L. Braunstein, H.J. Kimble and C.A. Fuchs, J. Mod. Opt. **47**, 267 (2000).  
 [12] K. Hammerer, M. M. Wolf, E. S. Polzik and J. I. Cirac, Phys. Rev. Lett. **94**, 150503 (2005).